

*Full Research Paper*

## **Ocean Color Inferred from Radiometers on Low-Flying Aircraft**

**James H. Churnside \* and James J. Wilson**

NOAA ESRL CSD3, 325 Broadway, Boulder, CO 80305, USA

E-mail: james.j.wilson@noaa.gov

\* Author to whom correspondence should be addressed. E-mail: james.h.churnside@noaa.gov

*Received: 16 November 2007 / Accepted: 5 February 2008 / Published: 8 February 2008*

---

**Abstract:** The color of sunlight reflected from the ocean to orbiting visible radiometers has provided a great deal of information about the global ocean, after suitable corrections are made for atmospheric effects. Similar ocean-color measurements can be made from a low-flying aircraft to get higher spatial resolution and to obtain measurements under clouds. A different set of corrections is required in this case, and we describe algorithms to correct for clouds and sea-surface effects. An example is presented and errors in the corrections discussed.

**Keywords:** ocean color, remote sensing, atmospheric correction, ocean optics

---

### **1. Introduction**

Ocean-color measurements from low-earth-orbiting satellites have proven to be a very important source of information about the global ocean. Of particular interest has been the concentration of chlorophyll-*a* in the upper ocean. This is a measure of the primary productivity of the upper layer, upon which most life in the sea depends.

The satellite instruments have problems for certain applications. One is that they cannot see the sea surface through clouds. Many of the most productive ocean regions are at high latitudes, where cloud cover is very common. The other is that the spatial resolution is too coarse to get good data very close to the shore. These coastal areas are also often very productive regions.

Ocean-color sensors on low-flying aircraft offer a way to fill in these gaps in the coverage from the satellite instruments. Before these data can be used in this way, atmospheric corrections must be applied that are different from those used to correct the satellite data. The most obvious difference is

the case where the aircraft is flying beneath clouds, and the illumination of the ocean is the diffuse illumination from the bottom of the cloud. The satellite instruments never make measurements under these illumination conditions.

Several authors have considered airborne measurements of ocean color with various atmospheric corrections. Guzzi, et al [1] used a clear sky atmospheric radiative transfer model and used the results with flights at altitudes of 1500 m and above. Zibordi et al [2] used a similar model, but flew as low as 150 m, which is closer to the altitudes of interest here. Harding et al [3] reported on the results of an extensive series of flights, but sun-glint removal was the only atmospheric correction used. Krottov and Vasilkov [4] considered the effects of an off-nadir, polarized radiance sensor to minimize surface reflection effects. They showed an increase in performance, but the azimuth angle between the receiver pointing direction and the sun becomes important. The receiver must track changes in aircraft heading and is more complex. Lavender and Nagur [5] flew at altitudes of 1500 m and 3000 m, and applied corrections for molecular scattering and aerosol scattering.

Lazin, et al [6] flew at altitudes of 150 and 300 m and in both clear and overcast conditions. They used a receiver very similar to ours, and our atmospheric correction uses a model that is similar to theirs. The main difference was that we measured downwelling irradiance, and they did not. That means that their atmospheric corrections relied on models of the sky light, while we assume that the downwelling irradiance is known.

We will consider the case where the downwelling irradiance and the upwelling radiance at nadir are measured from a low-flying aircraft. In Section 2, we describe a model for atmospheric corrections that includes contributions from sun glint, sun light reflected from foam on the surface, and skylight reflected from the surface in clear and overcast conditions. Section 3 provides an example of how the data were used to correct aircraft data. In Section 4, we discuss the sources and magnitudes of errors in the corrections, and suggest additional instrumentation to reduce those errors under certain conditions. Recommended additions are a down-looking video camera and an up-looking radiance sensor.

## 2. Reflectance Model

The remote sensing reflectance at an optical wavelength  $\lambda$  is defined as [7]:

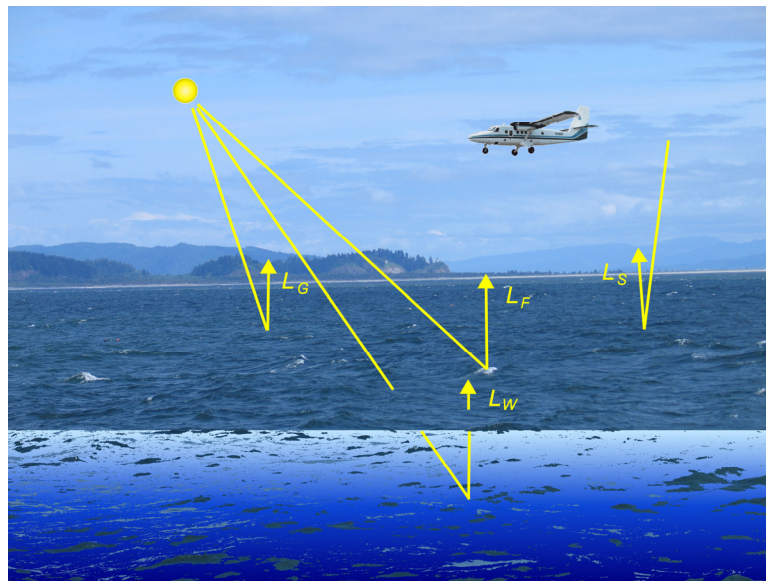
$$R_{RS}(\lambda) = \frac{L_w(\lambda)}{E(\lambda)}, \quad (1)$$

where  $L_w$  is the water-leaving radiance propagating in the zenith direction and  $E$  is the irradiance incident on the surface. Where multiple scattering in the atmosphere is negligible, the zenith-propagating radiance measured at the aircraft is the sum of the water leaving radiance and contributions from surface reflections. For each wavelength, this can be expressed as:

$$L = L_w + L_G + L_F + L_S, \quad (2)$$

where  $L_G$  is the radiance from sun glints,  $L_F$  is the radiance from foam on the surface, and  $L_S$  is the specular reflection of skylight from the surface. These contributions are shown schematically in Fig. 1.

**Figure 1.** Schematic of measurement geometry showing the four contributions to the zenith radiance in Eq. (2).



The radiance from sun glints can be approximated by

$$L_G = \frac{E_{SUN}(\phi)}{\cos \phi} R_F(\frac{1}{2}\phi) \frac{P(GLINT)}{\pi\alpha^2}, \quad (3)$$

where  $E_{SUN}$  is the direct solar irradiance at the surface,  $\phi$  is the solar zenith angle,  $R_F$  is the Fresnel reflection coefficient,  $P(GLINT)$  is the probability that a surface facet will reflect the sun into the field of view of the radiance sensor, and  $\alpha$  is the half angle of the field of view of the sensor, which is assumed to be circular.

The glint probability can be expressed in terms of the surface-slope statistics as:

$$P(GLINT) = \int_{\gamma_{x1}}^{\gamma_{x2}} \int_{\gamma_{y1}}^{\gamma_{y2}} d\gamma_y d\gamma_x p(\gamma_x, \gamma_y), \quad (4)$$

where the limits of integration depend on the solar angle and the field of view of the radiance sensor as follows:

$$\begin{aligned} \gamma_{x1} &= \tan^{-1} \left[ \frac{1}{2}(\phi - \alpha) \right] \\ \gamma_{x2} &= \tan^{-1} \left[ \frac{1}{2}(\phi + \alpha) \right] \\ \gamma_{y1} &= \tan^{-1} \left[ - \left( \alpha^2 - [2 \tan(\gamma_x) - \phi]^2 \right)^{\frac{1}{2}} \right] \\ \gamma_{y2} &= -\gamma_{y1}. \end{aligned} \quad (5)$$

The x direction is defined such that the solar azimuth angle is zero.

The probability density function of the surface slopes,  $p(\gamma_x, \gamma_y)$ , can be approximated by a zero-mean Gaussian with a mean-square slopes in the cross wind ( $\sigma_c^2$ ) and up/down ( $\sigma_u^2$ ) wind directions of [8, 9]

$$\begin{aligned}
\sigma_c^2 &= (1.42 - 2.8Ri)(0.003 + 0.00192U_{13.5}), & Ri < 0.27 \\
&= 0.65(0.003 + 0.00192U_{13.5}), & Ri > 0.27 \\
\sigma_u^2 &= (1.42 - 2.8Ri)0.00316U_{13.5}, & Ri < 0.27 \\
&= 0.65(0.00316U_{13.5}), & Ri > 0.27
\end{aligned} \tag{6}$$

where  $U_{13.5}$  is the wind speed at a measurement height of 13.5 m above the surface and  $Ri$  is a reduced Richardson number given by

$$Ri = g\Delta Tz / T_w U_z^2. \tag{7}$$

Here  $g$  is the acceleration due to gravity,  $\Delta T$  is the air/sea temperature difference,  $T_w$  is the water temperature, and  $U_z$  is the wind speed at a measurement height of  $z$ . For our purposes, we will neglect atmospheric stability effects and use  $Ri = 0$ . We will also neglect the along-wind/cross-wind asymmetry and use the average variance in both axes.

We estimate the solar zenith angle  $\phi$  using an approximation from Meeus [10] and the longitude, latitude, day of the year, and time of day. The details are presented in Appendix A.

To estimate the Fresnel reflection coefficient, we use the following approximation for the index of refraction of sea water:

$$n = 1.39855 - 1.64 \times 10^{-4} \lambda + 1.09 \times 10^{-7} \lambda^2, \tag{8}$$

where  $\lambda$  is the wavelength in nm. Over the range of wavelengths from 400 nm to 700 nm, our approximation to the index of refraction varies from 1.350 to 1.337, and the resulting values for the reflection at normal incidence from 0.0222 to 0.0208. For this wavelength range and a temperature range of 0 – 20° C, the maximum error in normal-incidence reflectivity produced by the use of this formula is about 0.5% of the true value calculated from the tabulated refractive indices of Austin and Halikas [7,11]. The Fresnel reflection coefficient for an incidence angle  $\beta$  is taken from Born and Wolf [12]:

$$R_F(\beta) = \frac{\tan^2 \left[ \beta - \sin^{-1} \left( \frac{\sin \beta}{n} \right) \right]}{2 \tan^2 \left[ \beta + \sin^{-1} \left( \frac{\sin \beta}{n} \right) \right]} + \frac{\sin^2 \left[ \beta - \sin^{-1} \left( \frac{\sin \beta}{n} \right) \right]}{2 \sin^2 \left[ \beta + \sin^{-1} \left( \frac{\sin \beta}{n} \right) \right]}. \tag{9}$$

The contribution from foam is estimated assuming that foam acts as a Lambertian reflector. The observed radiance can then be approximated as:

$$L_F = E_{SUN}(\phi) R_{FOAM} P(FOAM) / \pi, \tag{10}$$

where  $R_{FOAM}$  is the reflectivity of foam, and  $P(FOAM)$  is the probability encountering foam at any point on the surface. The reflectivity of foam depends on a number of factors, including thickness and

age. Whitlock, et al. [13] measured a maximum reflectivity of 0.55 for new, thick foam in the laboratory. Using this number as a calibration factor, Koepke [14] measured an average value for oceanic foam of 0.22. Frouin, et al. [15] made measurements in the surf zone, and obtained reflectivities of 0.2 to 0.6 out to about 650 nm, and decreasing values from there into the near infrared. Moore, et al. [16] measured the foam in a ship wake, and obtained a wide range of values up to 0.75, with decreasing reflectance at wavelengths longer than about 600 nm under all conditions. The measurement conditions of Koepke are the most similar to those of interest here, and we will use his results.

The fractional foam coverage,  $P(FOAM)$ , has also been measured a number of times. Using a least-squares fit to a number of data sets, Monahan and O'Muircheartaigh obtained the relationship [17]

$$P(FOAM) = 2.95 \times 10^{-6} U_{10}^{3.52}. \quad (11)$$

The exponent is close to the theoretical prediction [18] of 3.75, but does not include the effects of atmospheric stability. An approximation that includes parameterization of the atmospheric stability is [19]

$$P(FOAM) = 1.95 \times 10^{-5} U_{10}^{2.55} \exp(0.0861\Delta T). \quad (12)$$

The final term is the reflected sky radiance. This can be approximated by the product of the downwelling radiance near zenith and the Fresnel reflection coefficient at a normal incidence angle, which is

$$R_F(0) = \frac{(n-1)^2}{(n+1)^2}. \quad (13)$$

The downwelling radiance depends on whether the sky is clear or cloudy. For thick overcast, we can assume that the light coming from the bottom of the cloud is diffuse, so the radiance is simply the measured irradiance divided by  $\pi$  steradians. The effects of thin and broken clouds are considered in the discussion.

For clear skies, we can make an estimate based on Rayleigh scattering from atmospheric molecules. The scattering coefficient for a purely molecular atmosphere has been tabulated [20] for various wavelengths and heights. For heights up to 10 km and wavelengths from 300 to 900 nm, this table can be approximated by:

$$K_r = 2.07 \times 10^6 \exp(-1.12 \times 10^{-4} h) \lambda^{-4.1}, \quad (14)$$

where  $h$  is the height above the surface. The largest error in this approximation is 15.5%, 95% of the values are within 6.1%, and the median error is 1.8%. Note that pure Rayleigh scattering has a wavelength coefficient of -4. The difference is caused by the dispersion in the atmosphere.

The nadir-propagating radiance at the surface from molecular scattering can be estimated in a single-scattering approximation by

$$L_M = E_{SUN}(\phi) \int_0^{\infty} K_R(r) dr P(\phi), \quad (15)$$

where the integral is from the surface along the path of the incoming solar rays and  $P$  is the normalized Rayleigh phase function, given by

$$P(\phi) = \frac{\frac{3}{4}(1 + \cos^2 \phi)}{4\pi}. \quad (16)$$

To continue, we neglect the curvature of the Earth so that  $dr = \cos(\phi)dh$ . With this transformation, the integral in Eq. (15) can be evaluated, with the result

$$\begin{aligned} L_m &= E_{SUN}(\phi) \frac{1.84 \times 10^{10} \lambda^{-4.1}}{\cos \phi} \frac{\frac{3}{4}(1 + \cos^2 \phi)}{4\pi} \\ &= 1.1 \times 10^9 \left( \cos \phi + \frac{1}{\cos \phi} \right) \lambda^{-4.1} E_{SUN}(\phi). \end{aligned} \quad (17)$$

The reflection of this from the surface is subtracted to correct for the reflected skylight under clear-sky conditions.

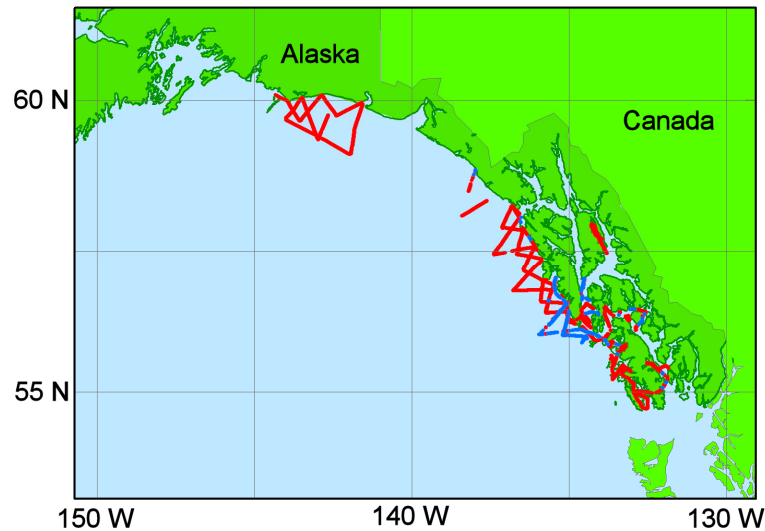
Light scattered by aerosols also contributes to the reflected skylight, but this contribution does not lend itself to simple parameterization. However, an estimate of marine aerosol scattering can be easily obtained using MODTRAN [21]. The aerosol model uses the sum of several lognormal aerosol size distributions whose parameters depend on current wind speed, wind speed averaged over the last 24 hours, and relative humidity [22]. Of course, MODTRAN also calculates the molecular scattering, and can be used to obtain an estimate for the total radiance at nadir from scattering in the atmosphere.

### 3. Example

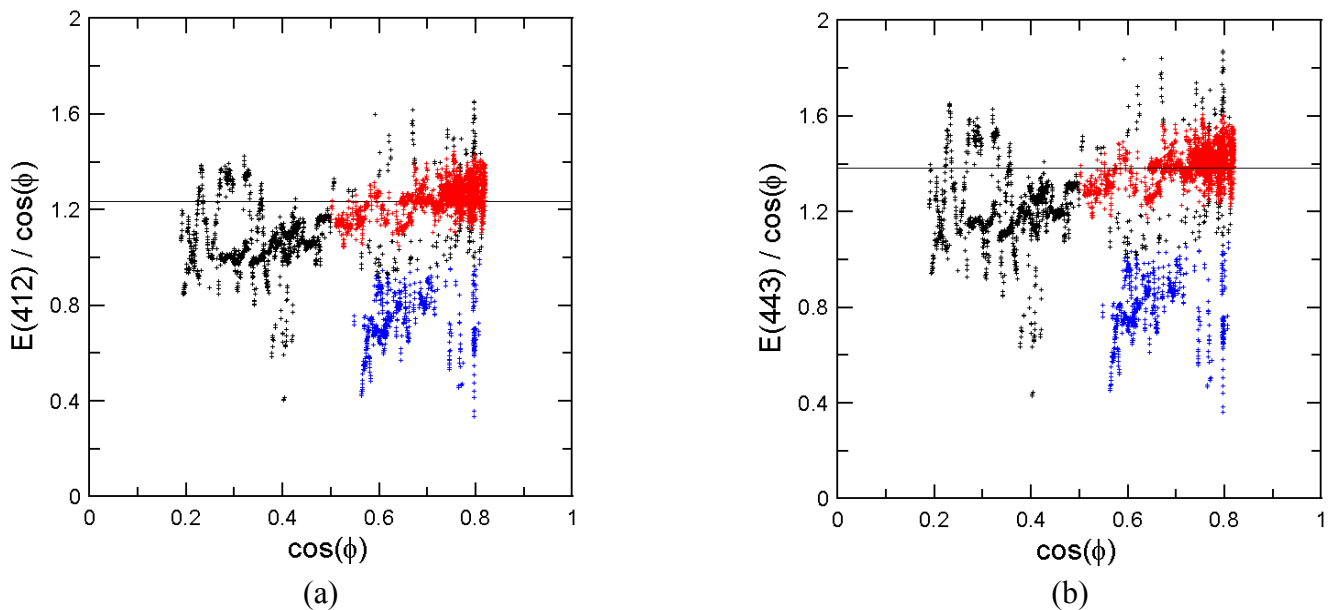
Ocean-color data were collected using a Satlantic MicroSAS radiometer suite with filters to approximate the Sea Viewing Wide Field of View Sensor (SeaWiFS) bands 1 – 7 (412, 443, 490, 510, 555, 670, and 765 nm). Filter bandwidths are 20 nm in the blue and green (bands 1 – 5) and 9 nm in the red and near infrared. The field of view of each radiance sensor was 52 mrad. Radiometers were mounted on the top of the aircraft to measure the downwelling irradiance and on the bottom to measure the upwelling radiance at similar wavelengths. The sensors were mounted on a Twin Otter aircraft and flown during a visual survey of small cetaceans in SE Alaskan waters (Fig. 2) between 19 May and 23 June 2003. The irradiance and radiance sensors were pointed at zenith and nadir, respectively. In addition, a video camera was installed looking down at the sea surface. Normal flight altitude was 150 m. Winds during the flights were low – generally, around  $2 \text{ m s}^{-1}$  or less. To process the data, we first averaged each sensor output over about 1 second and rejected data where the aircraft was banked and where the illumination was changing rapidly. To implement the first condition, we calculated the change in aircraft direction at each second using the three data points centered on the point of interest. If the change was greater than 0.05 radians, the central point was rejected. This threshold corresponds to a turn rate of  $0.05 \text{ rad s}^{-1}$ , or a bank angle of about  $15^\circ$  for the nominal flight speed of  $50 \text{ m s}^{-1}$ . To implement the second condition, we rejected a data point if the

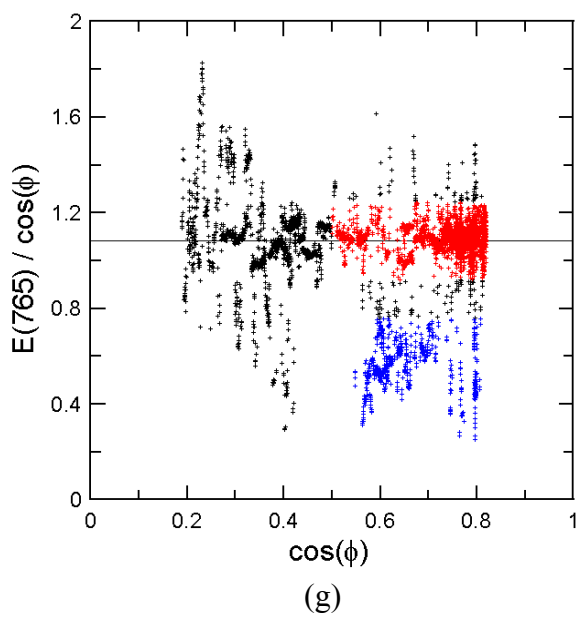
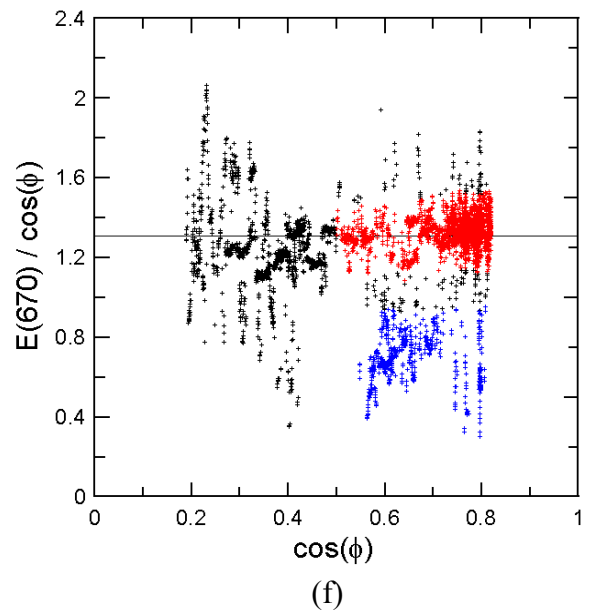
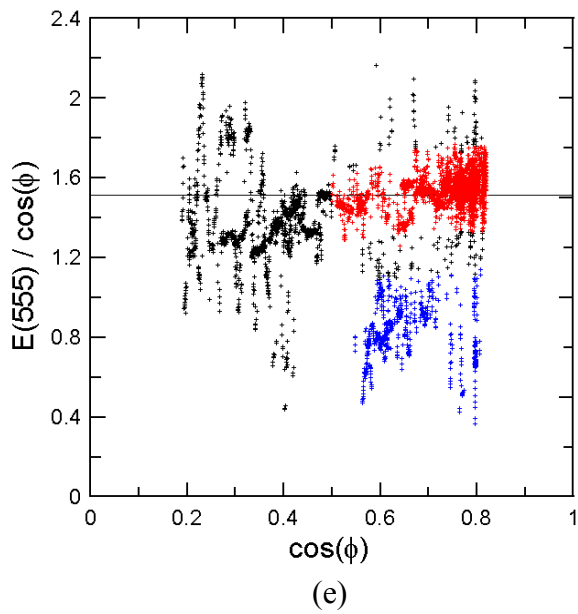
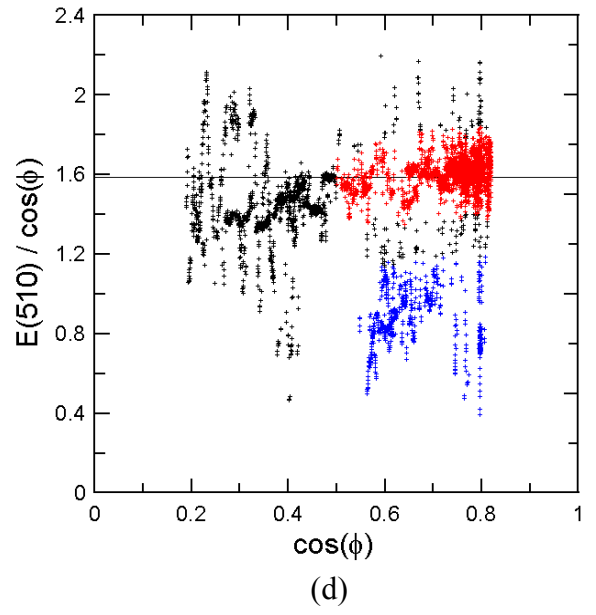
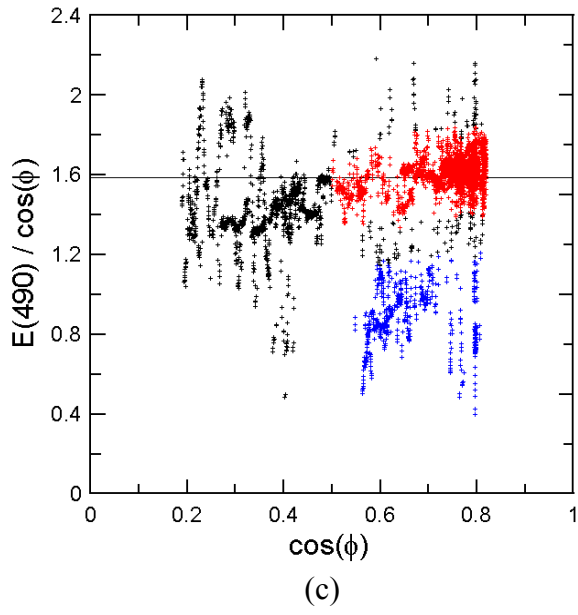
change in the irradiance in the center channel (509 nm) was different by more than 10% from the point before or the point after. All values of irradiance satisfying these conditions are plotted in Figure 3.

**Figure 2.** Chart of S.E. Alaska showing locations of clear (red) and cloudy (blue) measurements along flight tracks.



**Figure 3.** Measured downwelling irradiance  $E(\lambda)$  in  $W\ m^{-2}\ nm^{-1}$  divided by the cosine of the solar zenith angle  $\phi$ . Horizontal line represents the median value of all data. Black data points were rejected for reasons described in the text, so only the red (clear sky) and blue (cloudy sky) data points were used in the averaged spectra. a)  $\lambda = 412\ nm$ . b)  $\lambda = 443\ nm$ . c)  $\lambda = 490\ nm$ . d)  $\lambda = 510\ nm$ . e)  $\lambda = 555\ nm$ . f)  $\lambda = 670\ nm$ . g)  $\lambda = 765\ nm$ .





The next step was to separate the data collected under clear skies from those collected under cloudy skies. This was done using only the irradiance data in the red (781 nm) band. The sky was assumed to be clear if the normal-incidence irradiance (i.e., the measured irradiance divided by the cosine of the solar incidence angle) was within 15% of the median value of this quantity over all data. Since most of the flights were in clear-sky conditions, the median value was assumed to be a good representation of clear skies. It was assumed to be cloudy if the normal-incidence irradiance was below 70% of the median value. Data were not used if the normal-incidence irradiance was between 70% and 85% of the median; these were assumed to represent thin clouds for which the radiance at the bottom of the cloud may not be completely diffuse. Also, data were not used where the sun was within 30° of the horizon. Figure 3 shows the distribution of irradiance over sun angle; it generally follows the cosine of the sun angle except at the shorter wavelengths and low sun angles.

In the most basic atmospheric correction, we ignore foam and glint effects. For the clear data, we use the results from the previous section to get:

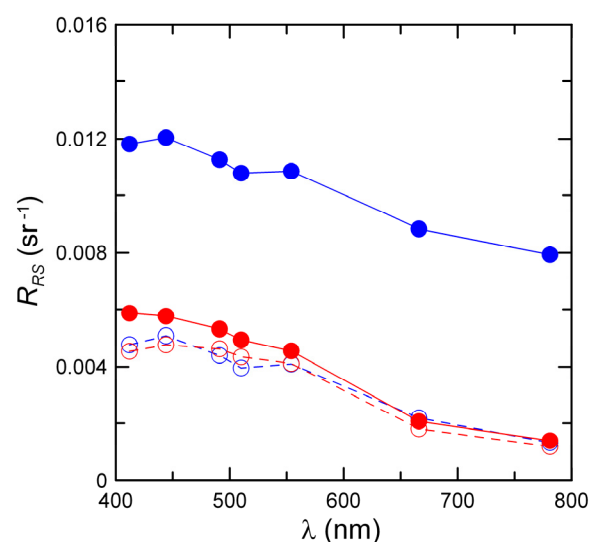
$$R_{RS}(\lambda) = \frac{L(\lambda) - R_F(0)L_S(\lambda)}{E(\lambda)}, \quad (17)$$

where  $L_S$  was estimated using MODTRAN with the sub-arctic summer model atmosphere, the maritime aerosol model, and both the current and 24 hour averaged winds set to 2 m s<sup>-1</sup>. For the cloudy data:

$$R_{RS}(\lambda) = \frac{L(\lambda)}{E(\lambda)} - \frac{R_F(0)}{\pi}. \quad (18)$$

Since these data collected during visual surveys, flights were only made during low-wind conditions for good visibility. These low winds also meant that there were few glints and foam patches, justifying the use of this basic correction. In a plot of the median values of the corrected reflectivities (Fig. 4),

**Figure 4.** Measured (solid circles) and corrected (open circles) remote sensing reflectance  $R_{RS}$  for clear (red) and overcast (blue) skies.



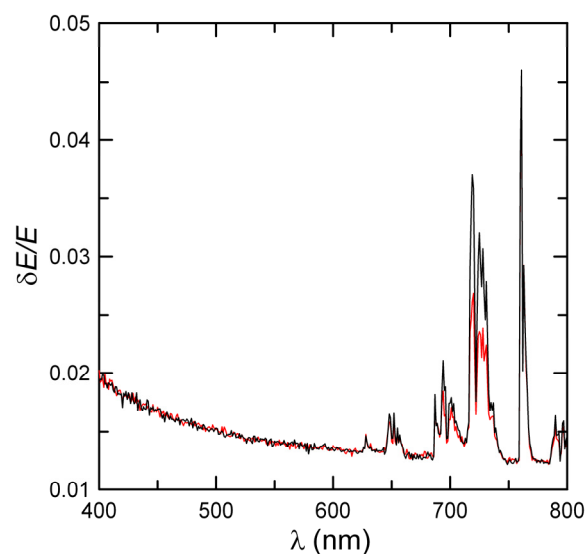
we see good overall agreement between the clear and cloudy cases, even though the correction for the cloudy cases is quite large. Since the clear and cloudy data were taken at different locations at different times, we would not necessarily expect them to be the same. However, Figure 2 shows that they had about the same mix of coastal and off-shore waters, so it is not too surprising that they are similar.

#### 4. Discussion

While the model described seems to provide a full correction for the remote sensing reflectance, it cannot be applied in all conditions. Estimates of the various contributions to the radiance are not exact, and the results become meaningless if the error in the correction is greater than the water-leaving radiance itself.

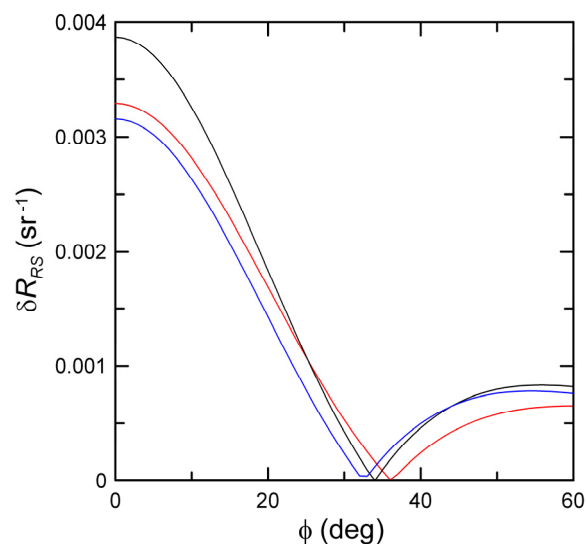
One obvious source of error arises from the assumption that the downwelling irradiance measured at the aircraft altitude is a good approximation to the downwelling irradiance at the surface. An example of the relative error can be estimated using MODTRAN to calculate the solar irradiance at the aircraft altitude and at the surface for a specific set of conditions. Fig. 5 presents results for the relative error as a function of wavelength for a solar zenith angle of  $30^\circ$ , an aircraft altitude of 150 m, clear skies, and the atmospheric models labeled as tropical and sub-arctic winter. Values for the mid-latitude summer, mid-latitude winter, and sub-arctic summer models lie between these extremes. The relative error is generally below 2%, except in the region of a water vapor absorption band around 720-730 nm and an  $O_2$  absorption at 760 nm. The water vapor absorption band is the only region where the five MODTRAN models differ significantly. The filters typically used for ocean-color measurements, of course, avoid these regions of the spectrum.

**Figure 5.** Relative error in estimate of surface irradiance  $\delta E/E$  produced by measuring irradiance at 150 m. Curves represent MODTRAN maritime models for tropical (black) and sub-arctic winter (red) atmospheres.



Perhaps the most difficult correction is that for glints. As an example, consider our nadir-viewing radiometers. Using the formulae in Section 2, we can estimate the error in the remote-sensing reflectance correction produced if the wind speed or air/sea temperature difference are not estimated accurately. At a wind speed of  $10 \text{ m s}^{-1}$  and no air/sea temperature difference, the standard deviation of surface tilt angles is about 15 degrees. The glint fraction in our receiver field of view varies from about 2% when the sun is at the zenith to about 0.1% for a solar zenith angle of  $60^\circ$ . The errors introduced by a  $\pm 1 \text{ m s}^{-1}$  error in estimated the wind speed and by a  $-0.5^\circ$  estimate of the air/sea temperature difference (Fig. 6) show similar patterns. The errors exceed  $0.001 \text{ sr}^{-1}$  until the solar zenith angle exceeds  $25^\circ$ . A minimum in the error occurs where the zenith angle is a little more than twice standard deviation of the surface tilt angle.

**Figure 6.** Estimated remote-sensing-reflectance error  $\delta R_{RS}$  for error in the glint correction caused by a  $1 \text{ m s}^{-1}$  error in estimating the wind speed (black), a  $0.5^\circ \text{ C}$  error in estimating air/sea temperature difference (red), and the uncertainty in the Cox-Munk model for surface-slope variance (blue) plotted as a function of the solar zenith angle  $\phi$ .



The error does not only depend on the uncertainty in estimating the model inputs, but also on the accuracy of the model itself. In [8] the reported uncertainties in the slope variances are  $0.002$  for  $\sigma_c^2$  and  $0.004$  for  $\sigma_u^2$ . The average error introduced by this range of uncertainty in the slope variances is also plotted in Fig. 6. The pattern and the magnitude are similar to that introduced by the uncertainty in parameter estimation discussed previously.

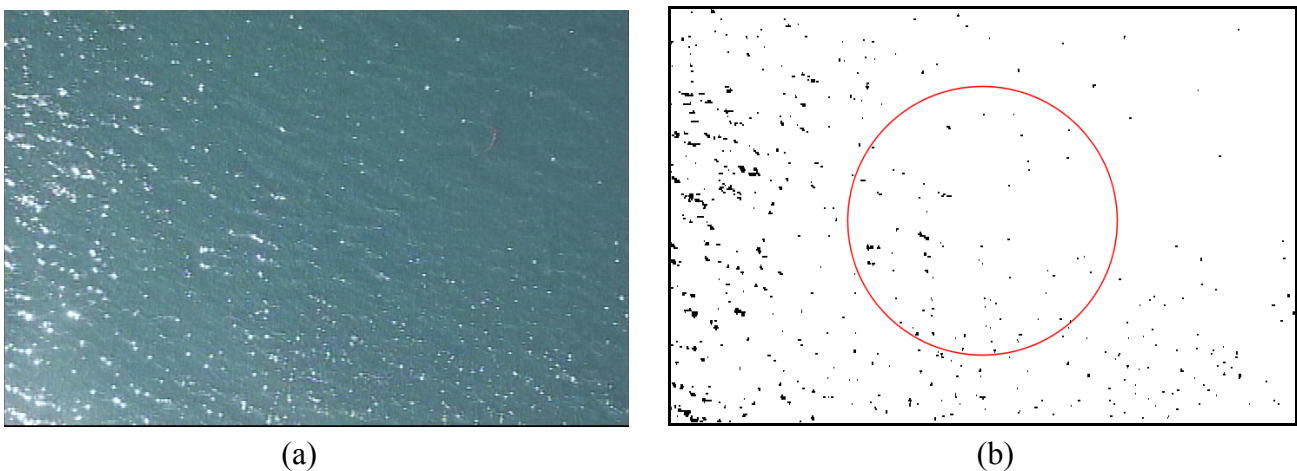
The foam correction is not as sensitive to errors in estimating the model parameters. Using Eq. (11) and a reflectivity of  $0.22$ , the correction to the remote sensing reflectivity for a wind speed of  $10 \text{ m s}^{-1}$  is only  $6.8 \times 10^{-4} \text{ sr}^{-1}$ . The error for a  $1 \text{ m s}^{-1}$  error in estimating the wind speed is  $2.4 \times 10^{-4} \text{ sr}^{-1}$ . The difference between the correction obtained from Eq. (11) and that obtained from Eq. (12) with  $\Delta T = 0$  is  $1.2 \times 10^{-4} \text{ sr}^{-1}$ . The error introduced by a  $1^\circ$  error in estimating the air/sea temperature difference in Eq. (12) is only  $4.2 \times 10^{-4} \text{ sr}^{-1}$ .

The models for foam coverage also represent data with a wide range of values. Consider, for example, figure 9 of Monahan and O'Muircheartaigh [17]. At a wind speed of  $10 \text{ m s}^{-1}$ , the measured

$P(\text{FOAM})$  values range from about 0.005 to about 0.05. For the value at the low end of this range, a correction using Eq. (12) would be too high by  $3.3 \times 10^{-4} \text{ sr}^{-1}$ ; for the value at the high end, the correction would be too low by 0.0035.

The discussion of the uncertainties in the corrections for glint and foam suggest that one might like to estimate  $P(\text{GLINT})$  and  $P(\text{FOAM})$  directly by imaging the surface. This can either be done with the same instrument that measures the ocean color (i.e., an imaging spectroradiometer) or, more simply, with a video camera that covers the field of view of the spectroradiometer. Fig 7 is an example of a video frame containing sun glints. Fig. 7a is the raw color image. We selected the red channel to obtain the greatest contrast and applied a threshold to select those pixels we identified as glints (a pixel value of 100 out of a maximum of 255 for this case). For the case of Fig. 7, the glint fraction is 0.0058, and the glint correction would be  $0.0137 \text{ sr}^{-1}$  or greater, depending on solar zenith angle. Actually, this image was taken when the aircraft was banked to point the radiometers closer to the sun and was not used in the estimation of the spectra in the previous section. It was included here as an example, because the images collected while the radiometers were looking in the nadir direction did not contain significant glints.

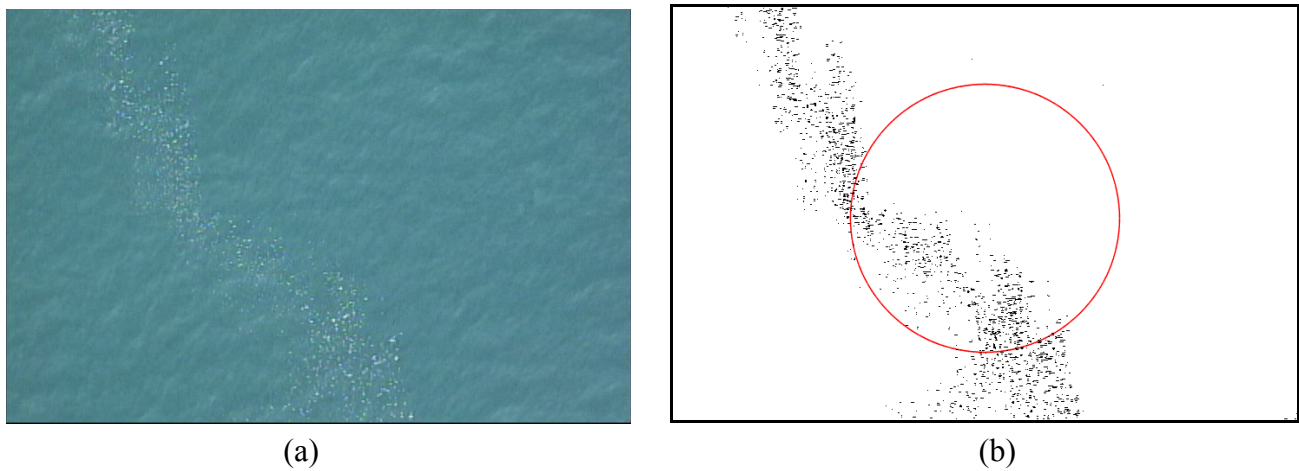
**Figure 7.** Video frame with sun glints. a) color image. b) negative of binary image with red circle denoting field of view of radiometers.



A similar analysis was done on a case with foam (Fig. 8). For this case, the foam fraction is 0.020, and the foam correction would be  $0.0014 \text{ sr}^{-1}$ . This was one of the highest foam fractions observed. In this case, the estimate based on wind speed would have predicted an extremely low foam fraction, since the foam was not generated by breaking waves, but by a strong horizontal current shear.

We found that the clear-sky correction was generally small. Fig. 9 presents a plot of the total correction for a zenith angle of  $30^\circ$ , and one sees it is generally below  $0.001 \text{ sr}^{-1}$ . Assuming that the error in the estimate is even lower, we do not expect a significant contribution to the error from this effect.

**Figure 8.** Video frame with foam. a) color image. b) negative of binary image with red circle denoting field of view of radiometers.



The error associated with uncertainties in the aerosol contribution is also small. We considered the case of a  $30^\circ$  solar zenith angle and a wind speed of  $10 \text{ m s}^{-1}$ . For this case, the error introduced in the remote sensing reflectance by a  $1 \text{ m s}^{-1}$  error in estimating wind speed would be about  $10^{-4} \text{ sr}^{-1}$  or less, depending on wavelength. The difference between mid-latitude summer and mid-latitude winter reflectance values was about  $10^{-4} \text{ sr}^{-1}$ , suggesting that the standard humidity profiles in MODTRAN are sufficient.

There are several sources of error associated with the cloud correction. The first is that the light leaving the bottom of a cloud is not perfectly diffuse [23, 24]. For an optically thick cloud, for example, the radiance distribution at the bottom is described by the escape function, which can be very roughly approximated by

$$K(\cos \theta) \approx \frac{1}{\pi}(0.4 + 0.9 \cos \theta), \quad (19)$$

where  $\theta$  is the zenith angle of observation. This is expected to be a reasonable approximation when the optical thickness is greater than about nine, the single-scatter albedo is one, and the single-scattering phase function is approximately Henyey-Greenstein with asymmetry parameter 0.85 [24]. Near zenith, this is about 30% greater than that predicted by the assumption of diffuse illumination. For clouds that are not optically thick, the illumination also depends on the position of the sun, and is much more complicated.

The second source of error enters in when the overcast is not uniform. The light collected by the irradiance sensor is weighted according to the cosine of the incidence angle, which means that the radiance from a point on the cloud separated by the receiver by a horizontal distance  $d$  is weighted according to

$$W_E = \frac{h_C - h_A}{\sqrt{(h_C - h_A)^2 + d^2}}, \quad (20)$$

where  $h_C$  and  $h_A$  are the cloud base and aircraft heights, respectively. This is the weighting function that goes into our estimate of the specularly reflected skylight. Actually, light from the bottom of the cloud will be reflected into the receiver if it encounters a surface facet at the appropriate angle to provide a specular reflection. This happens when the surface slope is in the same azimuth as the point of interest with a value of

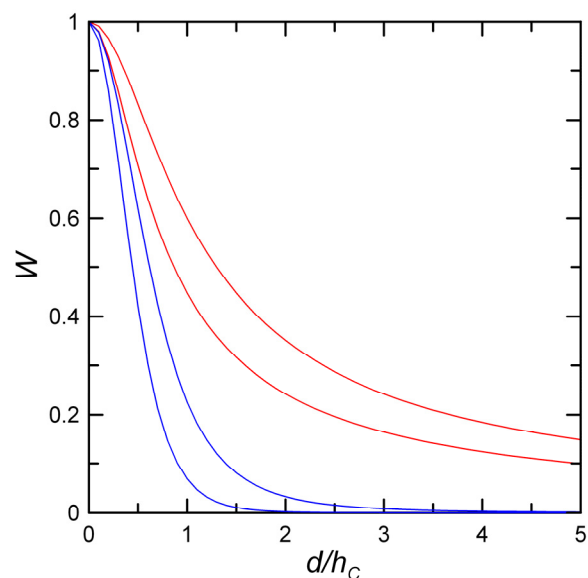
$$\gamma = \frac{\sqrt{d^2 + h_C^2} - h_C}{d}. \quad (21)$$

The corresponding weighting function is

$$W_L = \frac{(1 - \gamma^2)^2}{(1 + \gamma^2)} \exp\left(-\frac{\gamma^2}{2\sigma_\gamma^2}\right), \quad (22)$$

where the slope variance can be estimated from Eq. (7). Under typical conditions (Fig. 9), this drops off much more rapidly than the weighting function of irradiance. Very bright or dark regions of the cloud bottom away from the aircraft can produce an error in the estimate of reflected skylight based on the measured irradiance. This error is smaller if the aircraft is flying close to the cloud base, and the surface is rough.

**Figure 9.** Relative radiance weighting  $W$  of a point on the bottom of a cloud as a function of the horizontal distance from the receiver to that point  $d$  over the cloud base height  $h_C$  for the actual radiance reflected off the surface (blue) and the estimate from the measured irradiance (red). The upper and lower red curves correspond to an aircraft flight altitude of  $0.25h_C$  and  $0.5h_C$ , respectively. The upper and lower blue curves correspond to root-mean-square surface slopes of 0.3 (wind about  $20 \text{ m s}^{-1}$ ) and 0.2 (wind about  $9 \text{ m s}^{-1}$ ), respectively.



The error in the reflected skylight, especially under overcast conditions, suggests the implementation of a technique that has been used for near-surface measurements [25-27]. This involves an up-looking suite of radiometers to measure the sky radiance. Using the assumption that the radiance measured at zenith at the aircraft height is the same as that that would be measured at the surface, we can simply multiply this by the surface reflectance to get an estimate of the reflected skylight.

For near-surface measurements, the upwelling radiance is typically measured off nadir, and the downwelling radiance is measured at the same angle from zenith. For example, Mobley [26] suggests that the radiances be measured 40° from the nadir and zenith directions, both at an azimuth angle of 135° from the sun. There are two problems with this technique for aircraft operations. The first is that it may be difficult to maintain this orientation with respect to the sun if the aircraft is turning very often. The second is that the up-looking radiometer is not looking directly at the source of the reflected skylight. For a nadir angle of 40°, the horizontal separation is about 126 m. This can be significant if the skylight is not uniform, as for, example, under a variable overcast.

## 5. Conclusions

Accurate measurement of ocean color from a low-flying aircraft requires correction for the effects of sun glints, foam, and reflected skylight. Estimates of the first two corrections can be made using simple models based on surface wind speed, and the corrections can be reduced, or even eliminated, by making measurements under low-wind conditions. Glint and foam corrections can also be estimated by measuring glint fraction and foam coverage directly from video images of the surface. The correction for reflected skylight can also be estimated from models. For clear skies, aerosol contributions should be included, but the model does not need to be very accurate, because the magnitude of the correction is small. For cloudy skies, the correction is large, and a more accurate model is required. The contribution from thick, uniform clouds can be estimated by measuring the downwelling irradiance and assuming the light is diffuse. A more accurate estimate can be obtained by measuring the downwelling radiance directly.

We conclude that the best suite of instruments to measure ocean color from a low-flying aircraft would include three sets of radiometers at the colors of interest and a video camera. One radiometer set would measure downwelling irradiance to be used in the remote-sensing reflectance calculation. Another would measure upwelling radiance to be used for reflectance. The third would measure downwelling radiance to correct the measured upwelling radiance for the effects of reflected skylight in clear or cloudy conditions. The video would measure glint fraction and foam coverage to correct the measured upwelling radiance for the effects of glints and foam.

## Appendix A – Solar zenith angle

The solar zenith angle is calculated using the longitude, latitude, day of the year, and time of day [10]. First, the phase of the year, in radians, is calculated as:

$$\psi = \frac{2\pi}{365} \left( day - 1 + \frac{hour - 12}{24} \right) \quad (A1)$$

This is used to estimate the equation of time in minutes,

$$\begin{aligned} etime &= 229.18(0.000075 + 0.001868 \cos \psi - 0.032077 \sin \psi \\ &- 0.14615 \cos 2\psi - 0.040849 \sin 2\psi, \end{aligned} \quad (A2)$$

and the solar declination angle in radians

$$\begin{aligned} dec &= 0.006918 - 0.399912 \cos \psi + 0.070257 \sin \psi - 0.006758 \cos 2\psi \\ &+ 0.000907 \sin 2\psi - 0.002697 \cos 3\psi + 0.00148 \sin 3\psi. \end{aligned} \quad (A3)$$

The true solar time (minutes) is calculated using the longitude (degrees), the time zone used (hours from UTC), and the time of day as

$$tst = etime - 4lon + 60timezone + 60hour + minute. \quad (A4)$$

The solar hour angle (degrees) is

$$HA = 0.25tst - 180 \quad (A5)$$

The solar zenith angle is found from

$$\cos \phi = \sin(lat) \sin(dec) + \cos(lat) \cos(dec) \cos(HA) \quad (A6)$$

## Acknowledgements

Rod Hobbs of the NOAA Alaska Fisheries Science Center provided support for the measurements.

## References

1. Guzzi, R.; Rizzi, R.; Zibordi, G. Atmospheric correction of data measured by a flying platform over the sea: elements of a model and its experimental validation. *Appl. Opt.* **1987**, *26*, 3043-3051.
2. Zibordi, G.; Maracci, G.; Schlittenhardt, P. Ocean colour analysis in coastal waters by airborne sensors. *Int. J. Remote Sensing* **1990**, *11*, 705-725.
3. Harding, L. W. Jr.; Itsweire, E. C.; Esaias, W. E. Determination of phytoplankton chlorophyll concentrations in the Chesapeake Bay with aircraft remote sensing. *Remote Sens. Environ.* **1992**, *40*, 79-100.
4. Krotkov, N. A.; Vasilkov, A. P. Reduction of skylight reflection effects in the above-water measurement of diffuse marine reflectance: comment. *Appl. Opt.* **2000**, *39*, 1379-1381.
5. Lavender, S. J.; Nagur, C. R. C. Mapping coastal waters with high resolution imagery: atmospheric correction of multi-height airborne imagery. *J. Opt. A: Pure Appl. Opt.* **2002**, *4*, S50-S55.
6. Lazin, G.; Davis, R. F.; Ciotti, A. M.; Lewis, M. R. Ocean color measurements from low flying aircraft: Atmospheric and surface glint correction. *Proc. SPIE* **1997**, *2963*, 703-707.
7. Mobley, C. D. *Light and Water*; Academic Press: San Diego, 1994; pp. 70-86.

8. Cox, C.; Munk, W. Measurement of the roughness of the sea surface from photographs of the Sun's glitter. *J. Opt. Soc. Am.* **1954**, *44*, 838-850.
9. Shaw J. A.; Churnside, J. H. Scanning-laser glint measurements of sea-surface slope statistics. *Appl. Opt.* **1997**, *36*, 4202-4213.
10. Meeus, J. *Astronomical Algorithms*, 2<sup>nd</sup> Edition; Willmann-Bell: Richmond, Virginia, 1998; pp. 163-165.
11. Austin, R. W.; Halikas, G. The index of refraction of sea water. *SIO Ref. No. 76-1*; Scripps Institution of Oceanography: La Jolla, 1976; p. 121.
12. Born, M.; Wolf, E. *Principles of Optics*, 5<sup>th</sup> edition; Pergamon Press: Oxford, 1975; pp. 41-42.
13. Whitlock, C. H.; Barlett, D. S.; Gurganus, E. A. Sea foam reflectance and influence on optimum wavelength for remote sensing of ocean aerosols. *Geophys. Res. Lett.* **1982**, *9*, 719- 722.
14. Koepke, P. Effective reflectance of oceanic whitecaps. *Appl. Opt.* **1984**, *23*, 1816-1824.
15. Frouin, R.; Schwindling, M.; Deschamps, P.-Y. Spectral reflectance of sea foam in the visible and near-infrared: In situ measurements and remote sensing implications. *J. Geophys. Res.* **1996**, *101*, 14361-14371.
16. Moore, K. D.; Voss, K. J.; Gordon, H. R. Spectral reflectance of whitecaps: Instrumentation, calibration and performance in coastal waters. *J. Atmos. Ocean. Technol.* **1998**, *15*, 496-509.
17. Monahan, E. C.; O'Muircheartaigh, I. G. Optimal power-law description of oceanic whitecap coverage dependence on wind speed. *J. Phys. Oceanogr.* **1981**, *10*, 2094-2099.
18. Wu, J. Variations of whitecap coverage with wind stress and water temperature. *J. Phys. Oceanogr.* **1988**, *18*, 1448-1453.
19. Monahan, E. C.; O'Muircheartaigh, I. G. Whitecaps and the passive remote sensing of the ocean surface. *Int. J. Remote Sensing* **1986**, *7*, 627-642.
20. Wolfe, W. L.; Zissis, G. J. *The Infrared Handbook*; Environmental Research Institute of Michigan: Ann Arbor, 1978; pp. 4-38.
21. Berk, A.; Anderson, G. P.; Acharya, P. K.; Hoke, M. L.; Chetwynd, J. H.; Bernstein, L. S.; Shettle, E. P.; Matthew, M. W.; Alder-Golden, S. M. *MODTRAN4 Version 3 Revision 1 User's Manual*; Air Force Research Laboratory: Hanscom Air Force Base, MA, 2003; pp. 1-91.
22. Gathman, S. G. Optical properties of the marine aerosol as predicted by the Navy aerosol model. *Opt. Eng.* **1983**, *22*, 57-62.
23. King, M. D. Number of terms required in the Fourier expansion of the reflection function for optically thick atmospheres. *J. Quant. Spectrosc. Radiat. Transfer* **1983**, *30*, 143-161.
24. King, M. D. Determination of the scaled optical thickness of clouds from reflected solar radiation measurements. *J. Atmos. Sci.* **1987**, *44*, 1734-1751.
25. Carder, K. L.; Steward, R. G. A remote-sensing reflectance model of a red tide dinoflagellate off West Florida. *Limn. Oceanogr.* **1985**, *30*, 286-298.
26. Mobley, C. D. Estimation of the remote-sensing reflectance from above-surface measurements. *Appl. Opt.* **1999**, *38*, 7442-7455.
27. Hooker, S. B.; Lazin, G.; Zibordi, G.; McLean, S. An evaluation of above- and in-water methods for determining water-leaving radiances. *J. Atmos. Oceanic Technol.* **2002**, *19*, 486-515.